Chinese Physics Letters

LETTER

Chiral Floquet Selection of an Algebraic Rydberg Bound State in the Continuum

Cite as: X. Z. Zhang *et al*. 2026 *Chin. Phys. Lett.* **43** 110301

Recommended Articles

Tunable Topological Floquet Bound States in the Continuum in a Periodically Driven Double SSH Chain
Xian Duan, Ruozhen Wang, Bo Zhu, Zhi Tan, Honghua Zhong, and Shu Chen
Chin. Phys. Lett. **42**, 090601 (2025)

High-*Q* and Maximally Intrinsically Chiral Quasi-Bound States in the Continuum via Generative Adversarial Networks
Chen Zhong, Yi-Lin Wang, Jun-Wu Guo, E-Xian Liu, Jun Yi, Xin-Xing Zhou, and Jian-Jun Liu
Chin. Phys. Lett. **43**, 060401 (2026)

Bound States in the Continuum of Infinite Quality Factor in Finite Unit Cells
Hua-Wei Liang, Yuan-Zhi Liu, Yu-Jia Zeng, Yang-Jian Cai, and Ting-Yin Ning
Chin. Phys. Lett. **42**, 080401 (2025)

Quantum Simulation of Two-Dimensional U(1) Gauge Theory in Rydberg and Rydberg-Dressed Atom Arrays
Zheng Zhou, Zheng Yan, Changle Liu, Yan Chen, and Xue-Feng Zhang
Chin. Phys. Lett. **42**, 053705 (2025)

Floquet-Engineering Topological Phase Transition in Graphene Nanoribbons by Light
Anhua Huang, Shasha Ke, Ji-Huan Guan, Jun Li, and Wen-Kai Lou
Chin. Phys. Lett. **41**, (2024)

Robust Floquet-Induced Gap in Irradiated Graphite
Fei Wang, Xuanxi Cai, Wanying Chen, Jinxi Lu, Tianshuang Sheng, Xiao Tang, Jiansong Li, Hongyun Zhang, and Shuyun Zhou
Chin. Phys. Lett. **43**, 050705 (2026)

A series journal of Chinese Physical Society distributed by IOP Publishing

Chinese Physics Letters

Chin. Phys. Lett. **43** 110301 (2026)

LETTER

DOI: 10.1088/0256-307X/43/11/110301
CSTR: 32039.14.0256-307X.43.11.110301

Chiral Floquet Selection of an Algebraic Rydberg Bound State in the Continuum

X. Z. Zhang[1,2,*], X.-F. Zhang[3,*], and W.-M. Liu[1,4,*]

[1]College of Physics and Materials Science, Tianjin Normal University, Tianjin 300387, China
[2]Interdisciplinary Center, Tianjin Normal University, Tianjin 300387, China
[3]School of Physics & Information Science, Shaanxi University of Science and Technology, Xi'an 710021, China
[4]Beijing National Laboratory for Condensed Matter Physics, Institute of Physics, Chinese Academy of Sciences, Beijing 100190, China

[*]Corresponding authors. Email: zhangxz@tjnu.edu.cn; xfzhang@sust.edu.cn; wmliu@aphy.iphy.ac.cn

Bound states in the continuum remain localized despite the presence of extended modes at the same energy. In driven systems with long-range couplings, the absence of radiation does not by itself determine how a bound state decays in space. We study this problem in a Hermitian Rydberg spin waveguide, where a drive whose phase winds around a four-site plaquette combines rotation with time translation to exclude propagating guide channels from one symmetry sector. The resulting eigenstate remains embedded in the continuum of other sectors and carries an inverse-cube waveguide amplitude, with coherent contributions from direct plaquette–guide coupling and long-range guide propagation. Microscopic pair calculations determine the coupling in the axial Rydberg geometry, while coherent Floquet mixing accounts for the dominant angular-mode weight. The bound state thus retains the spatial signature of the long-range coupling even when radiation is forbidden.

Introduction

A bound state in the continuum (BIC) is a normalizable mode embedded in a spectrum of extended states [1–7]. Such states occur in wave and quantum systems in which coupling to a continuum does not necessarily lead to radiation [8–12]. Algebraically localized embedded states have also been demonstrated in engineered waveguide lattices [13], showing that embedding need not imply exponential localization. When the coupling to the continuum is long ranged, one must determine the spatial decay of the bound state as well as the condition for vanishing radiation.

Periodic driving makes the available radiation channels depend on both energy and harmonic index. Floquet BICs have been identified in periodically driven lattices [14]. Drive control of localization also appears in flux-induced wave-packet confinement in non-Hermitian rings [15] and in non-Hermitian Floquet edge modes [16]. Quasienergy folding creates continuum replicas, and the harmonic label can carry symmetry information in the enlarged Floquet space of Fourier components (Sambe space) [17–27]. A state can therefore share its quasienergy with extended modes while the symmetry sector labeled by its angular and Fourier indices contains no propagating guide channel. Rydberg arrays provide a microscopic setting for controlled spin Hamiltonians [28–32]. Individually controlled arrays realize prescribed geometries and correlated states [33–37]; resonant dipolar exchange supplies the long-range, angle-dependent coupling [38,39]; and periodic driving enables Hamiltonian engineering in isolated Rydberg spin systems [40]. Long-range interactions reshape the propagation of correlations and excitations [41–45]. Here the same long-range guide participates in the bound response even when symmetry excludes its propagating channels.

We consider a closed Hermitian system consisting of a winding-driven Rydberg plaquette coupled to an axial dipolar spin waveguide. The axial geometry supplies a long-range coupling with only the static angular component $\ell_s = 0$, while the winding factor changes the angular label seen by the continuum. Radiation is forbidden when the state's symmetry sector contains no propagating guide channel, but a bound state must also satisfy the real self-consistent eigenvalue equation. Its non-propagating guide response combines the direct plaquette–guide source with propagation through the long-range guide. The result is an algebraic Floquet BIC whose nonradiating waveguide amplitude follows $|\psi_n| \sim n^{-3}$. We determine the microscopic couplings using the Alkali Rydberg Calculator (ARC) [46,47] at the actual separations and angles. Floquet symmetry therefore excludes propagating replicas while coupling to the same dipolar continuum gives the bound state its spatial tail (Fig. 1).

Model and Floquet Selection

We work in the single-excitation sector of a four-site Rydberg plaquette coupled to a one-dimensional spin waveguide. The plaquette sites are labeled by angular coordinates $\theta_j = \pi j/2$, and the waveguide atoms are placed on an axis through the plaquette center. The four angular modes of the plaquette are labeled by $\ell = 0, \pm 1, 2$ modulo four. In the absence of driving the two circulating modes $\ell = \pm 1$ are degenerate, while the axial waveguide geometry selects a static plaquette-to-waveguide coupling vector with only $\ell_s = 0$ angular content. The drive is $H(t) = F(t)H_0F^{\dagger}(t)$, where H_0 is the static matrix and $F(t)$ multiplies plaquette site j by $\exp[\mathrm{i}\phi_j(t)]$, leaving the guide unchanged. Thus both internal plaquette links and plaquette–guide contacts acquire winding phases. The phase contains the prescribed terms $z_1 \sin(\Omega t - \theta_j + \varphi_1)$ and $(z_2/2)\sin(2\Omega t - 2\theta_j + \varphi_2)$, with parameters specified in the Supplementary Materials (SM), Section I. A Fourier component of the phase factor of order r, proportional to $\exp(\mathrm{i}r\Omega t - \mathrm{i}r\theta_j)$, carries angular index $-r$. If $J^{(0)}_{\ell_s n}$ denotes the static angular projection of the plaquette-to-site-n coupling, the continuum channel selected by this factor is

$$\ell_{\mathrm{eff}} = \ell_s - r \pmod 4. \tag{1}$$

For the axial geometry, the static channel is $\ell_s = 0$, while $r = 1$ couples to $\ell_{\mathrm{eff}} = -1$, as summarized in Fig. 1(b). The phase-factor order r is not the Floquet-state harmonic. With $u(t) = \sum_m u_m \exp(-\mathrm{i}m\Omega t)$, the joint rotation–time-translation label is $\kappa = m - \ell \pmod 4$. Its sector-resolved extended spectrum is

Received 9 July 2026; accepted 14 October 2026; published 4 November 2026

© 2026 Chinese Physical Society and IOP Publishing Ltd. All rights, including for text and data mining, AI training, and similar technologies, are reserved.

Check for updates

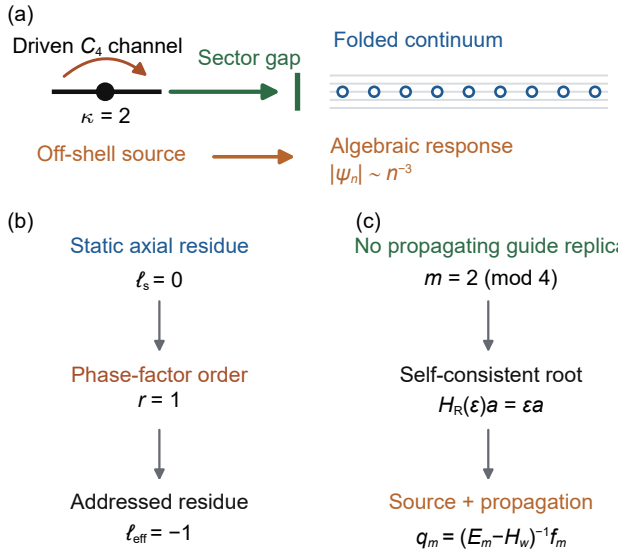

Fig. 1. Floquet symmetry separates radiation from the long-range bound response. (a) A winding-driven C_4 mode belongs to a joint sector whose accessible guide replicas are gapped even though other sectors form a folded continuum; the non-propagating coupling remains long ranged. (b) The axial static channel has $\ell_s = 0$, and phase-factor order $r = 1$ couples to the angular component $\ell_{\rm eff} = -1$. (c) The complete state, including its waveguide component, is nonradiating because no propagating guide replica is available in its $\kappa = 2$ sector, while its bound guide component obeys $q_m = (E_m - H_w)^{-1} f_m$. An embedded eigenstate must also satisfy the real self-consistent eigenvalue equation.

$$\sigma_{\rm ess}\left(H_{\rm F}^{(\kappa)}\right) = \bigcup_{m=\kappa\ (\mathrm{mod}\ 4)} (\mathcal{B} - m\Omega),$$

where $H_{\rm F}$ is the Floquet operator and $\mathcal{B}$ is the undriven guide band. For the parameters considered here, we identify an algebraically localized Floquet BIC belonging to the $\kappa = 2$ sector. We focus on this branch in the following discussion. Guide states have $\ell = 0$, so this state has accessible guide harmonics only at $m = 2$ (mod 4). Their physical sideband energies are $E_m = \epsilon + m\Omega$; the nearest allowed energies $E_{\pm 2}$ lie outside $\mathcal{B}$, whereas the in-band $m = 0, 1$ replicas belong to other sectors. The state can therefore be globally embedded while its own joint sector has no propagating guide replica. The Fourier-sign convention, the C_4 angular basis, and the static-channel projection are derived in the SM, Section III, and the Floquet-Feshbach conditions in Section II of the SM.

Within this state's symmetry sector, the angular weights follow from hybridization among levels coupled by the drive and shifted by the guide. Different angular components can therefore coexist at different harmonics of the same nonradiating Floquet state.

For the single-tone $L_w = 321$ state, the dominant components in the representation where the drive acts on site energies (the onsite representation) are $(\ell, m) = (2,0), (-1,1), (0,2)$. Their detunings are comparable to the drive coupling, so the eigenstate mixes these components rather than occupying only the addressed harmonic. Using the reference exchange scale J_* defined in SM, Section I, their bare Floquet energies are $0.5731J_*$, $-0.2478J_*$, and $-0.6443J_*$. The closed $m = 2$ guide block contributes a dispersive self-energy $0.3530J_*$, and the fundamental drive couples neighboring harmonics with magnitude $0.6655J_*$. The amplitudes $b_{\ell,m}$ and $a_{\ell,m}$ are the angular-harmonic components of $u_{\rm on} = F^\dagger u$ and u, respectively, and c_r is defined by $\exp[i\phi_j(t)] = \sum_r c_r \exp(ir\Omega t - ir\theta_j)$. Transforming the hybridized state back to the physical phase representation gives

$$a_{\ell,m} = \sum_r c_r b_{\ell+r,m+r}.$$

For $a_{-1,1}$, the three leading terms have magnitudes 0.2640, 0.1560, and 0.3159 with a common phase; including the remaining harmonics gives $|a_{-1,1}|^2 \simeq 0.61817$. The enhanced weight in the $\ell = -1$ angular mode and the absence of radiation therefore have different origins: coherent hybridization sets the former, whereas the joint symmetry excludes the propagating guide channels (SM, Section III and Fig. S1).

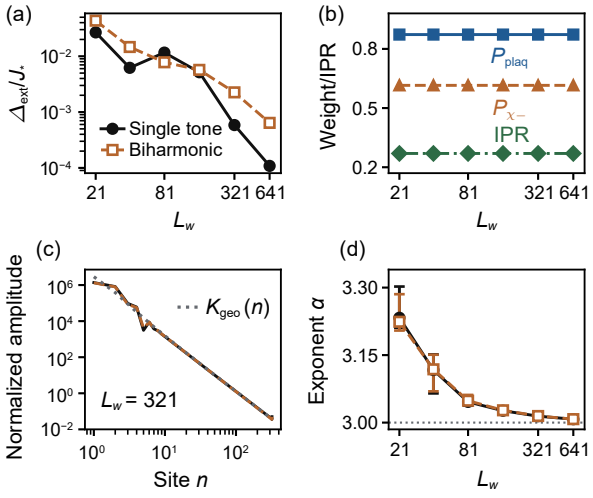

Fig. 2. Spectral proximity and algebraic localization of the same Floquet branch. (a) Periodic quasienergy distance $\Delta_{\rm ext}$ to the waveguide-like extended subset for the single-tone and biharmonic drives. (b) Plaquette weight, target-chirality weight, and IPR of the single-tone branch. (c) $L_w = 321$ snapshot amplitudes for both waveforms and the geometrical reference $K_{\rm geo}$, each normalized at $n = 108$; colors and markers follow panel (a). (d) Amplitude exponents fitted in interior window $\mathcal{W}_B$, with whiskers spanning windows $\mathcal{W}_A$–$\mathcal{W}_C$ of SM, Section VIII. The guide has open ends and uses $\Omega/J_* = 1.21$, $z_1 = 1.1$, and $z_2 = 0$ or 0.1.

Algebraic Embedded Branch

The Floquet modes are obtained from the unitary evolution over one drive period,

$$U(T)|u_\nu\rangle = \exp(-i\epsilon_\nu T)|u_\nu\rangle. \tag{2}$$

As the guide is extended, the same branch retains finite plaquette weight $P_{\rm plaq}$, target-chirality weight $P_{\chi-}$, and inverse participation ratio (IPR), while the waveguide-like folded spectrum becomes denser. The periodic quasienergy distance $\Delta_{\rm ext}$ measures its proximity to that extended subset [Figs. 2(a) and 2(b)]. The three local quantities are full-state snapshots at $t = 0$, defined in SM, Section I. The corresponding infinite-guide state lies in a gap of its own symmetry sector and in the continuum of other sectors (SM, Section IV).

Eliminating the waveguide with a Feshbach projection separates the radiation condition from the bound spatial response. An analogous energy-dependent self-energy reduction has been used for superconducting circuits coupled to structured waveguides [48]. In Floquet-Sambe space, let P and $Q = 1 - P$ project onto the plaquette and guide. The elimination gives a self-energy with Hermitian dispersive part $\Delta_{\rm F}$; the columns of $W_{\rm open}$ are the coupling vectors to independent propagating channels. With $H_{{\rm F},PP} = PH_{\rm F}P$, the localized component $|a_B\rangle = P|u_B\rangle$ of a BIC at quasienergy ϵ_B obeys

$$\begin{aligned} W_{\rm open}^\dagger(\epsilon_B)|a_B\rangle &= 0, \\ \left[H_{{\rm F},PP} + \Delta_{\rm F}(\epsilon_B)\right]|a_B\rangle &= \epsilon_B|a_B\rangle. \end{aligned} \tag{3}$$

The first line excludes radiation, while the second determines the self-consistent bound eigenstate. In the present construction, joint symmetry supplies the first condition by excluding every accessible propagating guide replica. The corresponding guide component obeys

$$(\epsilon_B - QH_{\rm F}Q)Q|u_B\rangle = QH_{\rm F}P|a_B\rangle. \tag{4}$$

The BIC condition removes the projection of the source $QH_{\rm F}P|a_B\rangle$ onto propagating outgoing modes, but it does not make the source vanish. Writing q_m and f_m for the guide response and contact source at harmonic m, one has $q_m = (E_m - H_w)^{-1} f_m$, with $E_m = \epsilon_B + m\Omega$. For a

uniform inverse-cube guide, the small-momentum dispersion contains a $k^2 \ln|k|$ nonanalyticity, giving an off-band full-line Green function $G_n^{\mathrm{line}}(E) \propto n^{-3}$. The response of the physical semi-infinite guide combines this long-range propagation with the direct plaquette–guide source, so both contributions enter the leading spatial coefficient. The derivation and its scope are given in the SM, Section V.

In the physical semi-infinite guide, the contact source and guide propagation enter the asymptotic response through two complex amplitudes. Here $\omega_w = (H_w)_{nn}$, $t_d = (H_w)_{n,n+d}$ is the real guide hopping, which depends only on the site separation, and $J_\infty = \lim_{d\to\infty} d^3 t_d$. For the nonoscillatory, absolutely summable response specified in SM, Section V, if $f_{n,m} = A_m n^{-3} + o(n^{-3})$ and $q_{n,m} = B_m n^{-3} + o(n^{-3})$, the off-band guide equation gives

$$\left(E_m - \omega_w - 2\sum_{d\geqslant 1} t_d\right) B_m = A_m + J_\infty \mathcal{M}_m,$$

$$\mathcal{M}_m = \sum_{n\geqslant 1} q_{n,m}.$$

The first term on the right is the direct contact source and the second is long-range propagation from the occupied guide sites near the plaquette. For the converged single-tone $L_w = 641$ state, the finite-guide ratios $J_\infty \mathcal{M}_m^{(L_w)}/A_m$, with $\mathcal{M}_m^{(L_w)} = \sum_{n=1}^{L_w} q_{n,m}$, are $+0.0896$ for $m = 2$ and -0.0484 for $m = -2$, showing that propagation can either reinforce or oppose the direct source. Exact cancellation of the two terms would remove the leading inverse-cube coefficient. The inverse-cube envelope is therefore a property of the source and guide response together, not of the geometrical reference alone (SM, Section V).

The computed Floquet profiles approach an inverse-cube envelope, consistent with the geometrical reference,

$$K_{\mathrm{geo}}(n) \equiv (R_{n_0}/R_n)^3 \sim n^{-3},$$
$$|\langle s_n | u_B(0)\rangle| \sim n^{-3} \quad (n \gg 1). \tag{5}$$

Here R_n is the plaquette-to-guide separation and n_0 is the normalization site, so K_{geo} is a distance-only reference; the Floquet source also depends on the harmonic amplitudes of the state, as derived in SM, Section V. The waveguide amplitude has the same leading power, so the corresponding probability is summable as n^{-6}. The exponent therefore reflects the combined dipolar source and guide response after radiation has been excluded by symmetry.

Figure 2 follows the same state spectrally and spatially. Its plaquette weight, target chirality, and IPR remain essentially unchanged over $L_w = 21$–641. At $L_w = 641$, the nearest extended-state spacings are $\Delta_{\mathrm{ext}}/J_* \simeq 1.09\times10^{-4}$ and 6.41×10^{-4} for the single-tone and biharmonic drives, respectively; the relation to the infinite-guide spectrum is derived in SM, Section IV. The amplitude exponent remains $\alpha = 3.006$–3.010 across three interior windows at this size (SM, Section VIII). The target chirality follows from coherent hybridization rather than from Eq. (1) alone: for the single-tone state, $P_{\chi_-}(0) \simeq 0.615$ and $\overline{P}_{\chi_-} \simeq 0.618$, with their small difference arising from interference between harmonics during a drive period (SM, Section III).

The connection between the finite-size branch and an infinite-guide eigenstate follows from the spectral residual, independently of proximity to finite-chain levels. Let $u_{L,M}$ be the normalized Floquet trial state in the onsite representation, set to zero outside the retained sites and harmonics, at $L = L_w = 641$ and harmonic cutoff $M = 16$, with finite-system quasienergy $\epsilon_{L,M}$. Self-adjointness gives

$$\mathrm{dist}\left\{\epsilon_{L,M}, \sigma\left[H_{\mathrm{F}}^{(\kappa)}\right]\right\} \leqslant \left\|\left[H_{\mathrm{F}}^{(\kappa)} - \epsilon_{L,M}\right] u_{L,M}\right\|.$$

For the two waveforms, the full infinite-operator residuals are bounded by $5.24\times10^{-7} J_*$ and $5.39\times10^{-7} J_*$, respectively, while the distance to the $\kappa = 2$ continuum exceeds $0.818 J_*$. Each residual interval lies within this sector's gap and inside the continuum of another sector. It therefore contains at least one eigenvalue of the specified effective operator with a normalizable eigenstate, while the same eigenvalue is embedded in the other-sector continuum (SM, Section IV). The chirality and spatial decay follow from the Floquet mode in Fig. 2 and the source–response analysis in Section V of the SM.

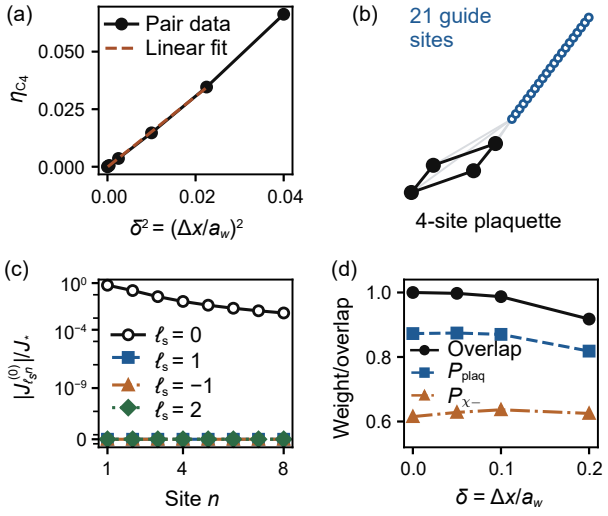

Fig. 3. Axial angular channel and its symmetry-breaking response. (a) A transverse displacement produces a quadratic onset of the unwanted-to-target static angular-channel power ratio η_{C_4}; the dashed line fits the small-displacement regime. (b) Schematic view of the 25-atom geometry, with the four-site plaquette enlarged for visibility. (c) At the axial point, the direct ARC exchange has a finite $\ell_s = 0$ component while the $\ell_s = \pm1, 2$ components vanish to numerical precision. (d) The finite Floquet branch remains continuously connected to the axial state over the plotted displacement range. Panels (a) and (c) use the static contacts to the first eight guide sites at $B = 20$ G; panel (b) shows the 25-atom geometry with a 21-site guide. The Floquet-state calculation in panel (d) uses $L_w = 161$, the same field, and the single-tone drive (SM, Section IX).

With the geometry, static exchanges, onsite terms, drive frequency, fundamental amplitude, and both phases fixed, the localized branch is followed at five values of z_2 between 0 and 0.1. The adjacent-state squared overlap remains above 0.99996 (SM, Section III), consistent with a continuous branch in this symmetry-preserving waveform family.

This is a Floquet form of symmetry protection: the conserved label combines rotation and time translation, so the state need not occupy a single angular mode at a fixed time. Unlike Friedrich–Wintgen cancellation between open resonant paths [4], the present joint sector has no propagating guide replica; the self-consistent real equation determines the embedded eigenstate within that sector.

Microscopic Geometry and Symmetry

The axial Rydberg geometry in Fig. 3 realizes the static angular channel used above. The selected 25-atom device has plaquette side $s \simeq 12.4128$ μm, axial offset $h \simeq 3.9489$ μm, and guide spacing $a_w \simeq 12.7781$ μm. All 300 pair exchanges are evaluated at their actual separations and angles with ARC [46,47], at $B = 20$ G. For the longer guides, the pair exchange is evaluated directly at each distinct separation and angle. The fixed-energy reduction, prescribed onsite terms, and full-precision geometry are specified in SM, Sections I, VI, and VII.

At the axial point, the four plaquette–guide contacts are equivalent and their static angular projection contains only $\ell_s = 0$. The $r = 1$ winding factor addresses $\ell_{\mathrm{eff}} = -1$ through Eq. (1), while the complete state retains the joint-sector radiation condition derived above. The signed, angle-dependent pair exchange supplies this angular structure in the effective spin model; both its direct contact source and the guide propagator enter the long-distance response.

The axial selection is exact at the level of the four contact amplitudes $C_{jn} = \langle p_j | H_0 | s_n \rangle$. If symmetry makes $C_{jn} = c_n^{(0)}$ independent of the plaquette site j, their angular projection is

$$J^{(0)}_{\ell_s n} = \frac{1}{2}\sum_{j=0}^{3} \exp(-\mathrm{i}\ell_s \pi j/2) C_{jn} = 2c_n^{(0)} \delta^{(4)}_{\ell_s,0}.$$

Here $\delta^{(4)}_{\ell_s,0}$ is one for $\ell_s = 0$ modulo four and zero otherwise. Thus the forbidden angular components vanish because of the geometry itself, while the pair calculation fixes the signed magnitude of the surviving contact. A transverse shift $\delta = \Delta x/a_w$ destroys this equivalence. Reflection symmetry groups the displaced contacts as (a_n, b_n, b_n, a_n), where a_n, b_n denote static contact amplitudes, not Floquet-state coefficients. For a smoothly varying pair exchange with nonzero axial coupling, the ratio of unwanted to target angular-channel power reduces to

$$\eta_{C_4}(\delta) = \frac{\sum_{n=1}^{8} |a_n(\delta) - b_n(\delta)|^2}{\sum_{n=1}^{8} |a_n(\delta) + b_n(\delta)|^2} = c_\delta \delta^2 + O(\delta^4).$$

The sums cover the same eight guide sites as Fig. 3(a), and c_δ is the quadratic coefficient at the axial point. Reversing δ exchanges a_n and b_n, so both powers are even and the next correction is fourth order. The quadratic onset in Fig. 3(a) therefore follows from the breaking of the angular selection rule (SM, Sections VII and IX).

The static angular mixing is accompanied by a continuous evolution of the finite Floquet state from its axial reference over the plotted range, with squared overlap with the axial state 0.918 at $\delta = 0.20$ [Fig. 3(d)]. The complete displacement dependence is given in SM, Section IX; the infinite-guide BIC statement applies to the symmetry-preserving axial geometry.

Discussion

An embedded state can remain nonradiating while retaining an algebraic response to the long-range continuum. Radiation exclusion and spatial localization are separate conditions: the joint Floquet symmetry removes the propagating guide channels accessible to the state, while the Hermitian eigenproblem fixes the bound solution. The remaining dipolar response combines direct contact coupling and propagation through the guide, producing the algebraic envelope of that same state. Coherent Floquet hybridization determines its chirality, and the axial Rydberg geometry supplies the required static angular channel.

The waveform deformation preserves the combined symmetry and hence the allowed guide harmonics, whereas transverse displacement admits angular components excluded on the axis. This distinction does not depend on the particular Rydberg parameters used here. In a driven long-range continuum, symmetry can forbid the propagating channels at the state's quasienergy while coupling to the remaining guide modes still produces a spatial tail. The source and propagation through the guide together determine that tail. Whether a self-consistent embedded eigenstate exists and which power law survives depend on the system. The spatial decay of a Floquet BIC can therefore reveal how long-range coupling acts even when radiation is forbidden.

Acknowledgements

This work was supported by the National Natural Science Foundation of China (Grant Nos. 12275193 and 12675024 for X.Z.Z., Grant No. 12475004 for X.-F.Z., and Grant Nos. 12334012, 12234012, and 52327808 for W.-M.L.), the National Key R&D Program of China (Grant Nos. 2024YFF0726700, 2021YFA1400900, and 2021YFA0718300 for W.-M.L.), the Youth Innovation Team of Shaanxi Universities (for X.-F.Z.), the Space Application System of China Manned Space Program (for W.-M.L.), and the Elite Revitalizing Inner Mongolia Program (Grant No. 2025TGL05 for W.-M.L.).

Data Availability

The data and scripts that support the figures are available from the corresponding authors upon reasonable request.

References

[1] von Neumann J and Wigner E P 1929 *Phys. Z.* **30** 465
[2] Fano U 1961 *Phys. Rev.* **124** 1866
[3] Stillinger F H and Herrick D R 1975 *Phys. Rev. A* **11** 446
[4] Friedrich H and Wintgen D 1985 *Phys. Rev. A* **32** 3231
[5] Miroshnichenko A E, Flach S, and Kivshar Y S 2010 *Rev. Mod. Phys.* **82** 2257
[6] Hsu C W, Zhen B, Stone A D, Joannopoulos J D, and Soljačić M 2016 *Nat. Rev. Mater.* **1** 16048
[7] Sadreev A F 2021 *Rep. Prog. Phys.* **84** 055901
[8] Fan S and Joannopoulos J D 2002 *Phys. Rev. B* **65** 235112
[9] Marinica D C, Borisov A G, and Shabanov S V 2008 *Phys. Rev. Lett.* **100** 183902
[10] Plotnik Y, Peleg O, Dreisow F, Heinrich M, Nolte S, Szameit A, and Segev M 2011 *Phys. Rev. Lett.* **107** 183901
[11] Yang Y, Peng C, Liang Y, Li Z, and Noda S 2014 *Phys. Rev. Lett.* **113** 037401
[12] Koshelev K, Favraud G, Bogdanov A, Kivshar Y, and Fratalocchi A 2019 *Nanophotonics* **8** 725
[13] Corrielli G, Della Valle G, Crespi A, Osellame R, and Longhi S 2013 *Phys. Rev. Lett.* **111** 220403
[14] Longhi S and Della Valle G 2013 *Sci. Rep.* **3** 2219
[15] Zhang X Z and Song Z 2019 *Phys. Rev. A* **99** 012113
[16] Zhang X and Gong J 2020 *Phys. Rev. B* **101** 045415
[17] Shirley J H 1965 *Phys. Rev.* **138** B979
[18] Sambe H 1973 *Phys. Rev. A* **7** 2203
[19] Grifoni M and Hänggi P 1998 *Phys. Rep.* **304** 229
[20] Bukov M, D'Alessio L, and Polkovnikov A 2015 *Adv. Phys.* **64** 139
[21] Goldman N and Dalibard J 2014 *Phys. Rev. X* **4** 031027
[22] Eckardt A and Anisimovas E 2015 *New J. Phys.* **17** 093039
[23] Eckardt A 2017 *Rev. Mod. Phys.* **89** 011004
[24] Lignier H, Sias C, Ciampini D, Singh Y, Zenesini A, Morsch O, and Arimondo E 2007 *Phys. Rev. Lett.* **99** 220403
[25] Jotzu G, Messer M, Desbuquois R, Lebrat M, Uehlinger T, Greif D, and Esslinger T 2014 *Nature* **515** 237
[26] Oka T and Kitamura S 2019 *Annu. Rev. Condens. Matter Phys.* **10** 387
[27] Rudner M S and Lindner N H 2020 *Nat. Rev. Phys.* **2** 229
[28] Saffman M, Walker T G, and Mølmer K 2010 *Rev. Mod. Phys.* **82** 2313
[29] Weimer H, Müller M, Lesanovsky I, Zoller P, and Büchler H P 2010 *Nat. Phys.* **6** 382
[30] Saffman M 2016 *J. Phys. B* **49** 202001
[31] Browaeys A and Lahaye T 2020 *Nat. Phys.* **16** 132
[32] Morgado M and Whitlock S 2021 *AVS Quantum Sci.* **3** 023501
[33] Labuhn H, Barredo D, Ravets S, de Léséleuc S, Macrì T, Lahaye T, and Browaeys A 2016 *Nature* **534** 667
[34] Barredo D, de Léséleuc S, Lienhard V, Lahaye T, and Browaeys A 2016 *Science* **354** 1021
[35] Endres M, Bernien H, Keesling A, Levine H, Anschuetz E R, Krajenbrink A, Senko C, Vuletic V, Greiner M, and Lukin M D 2016 *Science* **354** 1024
[36] Bernien H, Schwartz S, Keesling A, Levine H, Omran A, Pichler H, Choi S, Zibrov A S, Endres M, Greiner M, Vuletić V, and Lukin M D 2017 *Nature* **551** 579
[37] Omran A, Levine H, Keesling A, Semeghini G, Wang T T, Ebadi S, Bernien H, Zibrov A S, Pichler H, Choi S, Cui J, Rossignolo M, Rembold P, Montangero S, Calarco T, Endres M, Greiner M, Vuletic V, and Lukin M D 2019 *Science* **365** 570
[38] de Léséleuc S, Barredo D, Lienhard V, Browaeys A, and Lahaye T 2017 *Phys. Rev. Lett.* **119** 053202
[39] Ravets S, Labuhn H, Barredo D, Lahaye T, and Browaeys A 2015 *Phys. Rev. A* **92** 020701(R)
[40] Geier S, Thaicharoen N, Hainaut C, Franz T, Salzinger A, Tebben A, Grimshandl D, Zürn G, and Weidemüller M 2021 *Science* **374** 1149
[41] Hauke P and Tagliacozzo L 2013 *Phys. Rev. Lett.* **111** 207202
[42] Jurcevic P, Lanyon B P, Hauke P, Hempel C, Zoller P, Blatt R, and Roos C F 2014 *Nature* **511** 202
[43] Richerme P, Gong Z X, Lee A, Senko C, Smith J, Foss-Feig M, Michalakis S, Gorshkov A V, and Monroe C 2014 *Nature* **511** 198
[44] Foss-Feig M, Gong Z X, Clark C W, and Gorshkov A V 2015 *Phys. Rev. Lett.* **114** 157201
[45] Gong Z, Guaita T, and Cirac J I 2023 *Phys. Rev. Lett.* **130** 070401
[46] Šibalić N, Pritchard J D, Adams C S, and Weatherill K J 2017 *Comput. Phys. Commun.* **220** 319
[47] Robertson E J, Šibalić N, Potvliege R M, and Jones M P A 2021 *Comput. Phys. Commun.* **261** 107814
[48] Zhou J, Zhang X X, and Zhang X Z 2026 *Phys. Rev. A* **113** 062466